

Bridging Network Fragmentation: A Semantic-Augmented DRL Framework for UAV-aided VANETs

Gaoxiang Cao, Wenke Yuan, Huasen He, *Member, IEEE*, Yunpeng Hou, Xiaofeng Jiang, *Member, IEEE*,
Shuangwu Chen, *Member, IEEE*, Jian Yang, *Senior Member, IEEE*

Abstract—Vehicular Ad-hoc Networks (VANETs) are the digital cornerstone of autonomous driving, yet they suffer from severe network fragmentation in urban environments due to physical obstructions. Unmanned Aerial Vehicles (UAVs), with their high mobility, have emerged as a vital solution to bridge these connectivity gaps. However, traditional Deep Reinforcement Learning (DRL)-based UAV deployment strategies lack semantic understanding of road topology, often resulting in blind exploration and sample inefficiency. By contrast, Large Language Models (LLMs) possess powerful reasoning capabilities capable of identifying topological importance, though applying them to control tasks remains challenging. To address this, we propose the Semantic-Augmented DRL (SA-DRL) framework. Firstly, we propose a fragmentation quantification method based on Road Topology Graphs (RTG) and Dual Connected Graphs (DCG). Subsequently, we design a four-stage pipeline to transform a general-purpose LLM into a domain-specific topology expert. Finally, we propose the Semantic-Augmented PPO (SA-PPO) algorithm, which employs a Logit Fusion mechanism to inject the LLM’s semantic reasoning directly into the policy as a prior, effectively guiding the agent toward critical intersections. Extensive high-fidelity simulations demonstrate that SA-PPO achieves state-of-the-art performance with remarkable efficiency, reaching baseline performance levels using only 26.6% of the training episodes. Ultimately, SA-PPO improves two key connectivity metrics by 13.2% and 23.5% over competing methods, while reducing energy consumption to just 28.2% of the baseline.

Index Terms—UAV-assisted VANETs, Deep Reinforcement Learning, Large Language Models, Network Connectivity, Semantic Augmentation

I. INTRODUCTION

WITHIN the ambitious framework of sixth-generation (6G) mobile communications and Intelligent Transportation Systems (ITS), wireless connectivity characterized by ubiquitous coverage, ultra-low latency, and high reliability is regarded as the fundamental digital infrastructure for enabling Level 4/Level 5 (L4/L5) autonomous driving [1]. As the medium for information exchange in Vehicle-to-Vehicle (V2V) and Vehicle-to-Infrastructure (V2I) communications, Vehicular Ad-Hoc Networks (VANETs) undertake critical tasks, including cooperative sensing, traffic condition warnings, and computation offloading [2]. However, the physical characteristics

of modern urban canyons constitute a substantial barrier to wireless wave propagation. High-density building complexes induce severe shadow fading [3], while the high mobility of vehicles causes the network topology to fluctuate drastically on a time scale of seconds [4]. This dual spatiotemporal dynamicity frequently leads to network partitioning into isolated fragmented subnets [5], creating fragmented systems that severely constrain the continuity and safety of Internet of Vehicles (IoV) services.

Although traditional terrestrial Roadside Unit (RSU) deployment constitutes the network backbone, it is constrained by construction costs and land resources, making it difficult to achieve seamless coverage in all blind zones [6]. Furthermore, fixed infrastructure lacks resilience, particularly in scenarios involving sudden traffic congestion or disasters [7]. In this context, Unmanned Aerial Vehicles (UAVs), functioning as aerial base stations or mobile relays, have emerged as an ideal remedial solution for enhancing VANET connectivity [8]. This is attributed to their high probability of establishing Line-of-Sight (LoS) communication links [9] and their flexible three-dimensional maneuverability. UAV with high mobility is capable of dynamically tracking ground traffic hotspots and repairing broken links in real-time, thereby constructing a resilient air-ground integrated network architecture.

However, controlling UAV nodes to dynamically track and bridge the most critical disconnected areas on the ground under limited onboard energy constraints, thereby maximizing overall network connectivity, represents a typical non-convex, non-linear, and highly dynamic optimization problem [10]. Traditional UAV path planning methods, such as Mixed Integer Linear Programming (MILP), convex optimization, or heuristic algorithms based on potential fields, often rely on precise prior knowledge of environmental models. Furthermore, they suffer from excessive computational complexity when confronting high-dimensional state spaces and real-time dynamic variations, making it difficult to satisfy the real-time requirements of VANETs [11]. In recent years, Deep Reinforcement Learning (DRL) has gradually become a mainstream approach for addressing UAV dynamic deployment problems, owing to its end-to-end decision-making capabilities and adaptability to unknown environments [12]. Specifically, the Proximal Policy Optimization (PPO) algorithm [13] has been widely applied in UAV attitude control and trajectory planning due to its stability in continuous control tasks, sample efficiency, and robustness to hyperparameters [14].

G. Cao, W. Yuan, H. He, Y. Hou, X. Jiang, S. Chen and J. Yang are with the Department of Automation, University of Science & Technology of China. H. He (hehuasen@ustc.edu.cn) and Y. Hou (hyp314@mail.ustc.edu.cn) are the corresponding authors.

The source code will be publicly available upon acceptance.

On the other hand, the explosive development of Large Language Models (LLMs) over the past two years has provided novel perspectives for the dynamic deployment of UAVs [15], [16]. LLMs, pre-trained on massive textual datasets, have not only mastered natural language processing capabilities but have also demonstrated emergent abilities in Commonsense Reasoning, Spatial Planning, and Causal Inference [17]. Research indicates that LLMs are capable of comprehending textual descriptions of environments and generating rational action recommendations or sequences of sub-goals based on common sense [18]. This suggests that LLMs can serve as high-level planners or knowledge bases to guide DRL agents in complex decision-making tasks. For instance, LLMs can provide prior knowledge about urban layouts, traffic patterns, and UAV operational constraints, which can be integrated into the DRL framework to enhance learning efficiency and policy performance. Therefore, we propose integrating the semantic reasoning capabilities of LLMs into the decision-making process of UAVs. Our objective is to endow the agent with topological priors, enabling it to intelligently identify critical connectivity hubs, thereby maximizing network coverage while minimizing energy consumption.

A. Related Works

1) *Connectivity of UAV Aided VANETs*: Existing research has achieved notable progress in UAV-aided VANETs, particularly regarding VANET connectivity. In [19], VANET connectivity under varying vehicle densities was investigated by employing fast global k-means (FGKMs)-based vehicles clustering (FGVC) and the interior penalty function method (IPM) to approximately maximize the data transmission rate while simultaneously minimizing energy consumption and latency. Similarly, a drone-assisted cooperative routing (DACR) protocol was designed in [20] that integrates the Internet of Things (IoT) to enhance connectivity and data exchange capabilities within VANETs in dynamic, high-density environments. Furthermore, the augmentation of Roadside Units (RSUs) by equipping UAVs with Dedicated Short-Range Communications (DSRC) transceivers was proposed in [21], which improved the network coverage of VANETs through the construction of Voronoi diagrams. To address the dynamicity of UAV network topologies, the study in [22] designed a delay-constrained time-varying graph (DTVG) and proposed a novel data dissemination algorithm, thereby enhancing network connectivity and throughput. However, a critical limitation persists in these studies: the majority of existing works model the UAV deployment area either as a continuous Euclidean space or simplify it into a grid-based rasterized representation. Such abstractions fundamentally neglect the topological constraints inherent to urban mobility—specifically, that vehicular movement is strictly confined to road networks rather than being freely distributed across a planar surface. Consequently, these approaches may fail to capture the complex connectivity relationships among fragmented vehicle clusters. Moreover, while metrics based on distance or Signal-to-Interference-plus-Noise Ratio (SINR) are effective for evaluating local link quality, they are insufficient for characterizing the fragmentation state

of the global network. To address these challenges, we propose a graph-theoretic modeling approach to rigorously quantify connectivity and guide agents toward topologically critical intersections.

2) *UAV Deployment Using DRL Methods*: Extensive efforts have been made in existing literature to apply DRL methods to UAV deployment problems. For instance, a DRL-based algorithm was proposed in [23] for complex scenarios involving multiple obstacles and dependent tasks represented by Directed Acyclic Graphs (DAGs), achieving joint optimization of UAV trajectory planning, task scheduling, and Service Function (SF) deployment. Similarly, the study in [24] presented a DRL scheme based on Dueling Double DQN (D3QN) to jointly optimize bandwidth allocation, UAV 3D coordinates, and the phase shifts of Reconfigurable Intelligent Surfaces (RIS). Concurrently, researchers have attempted to apply DRL to UAV trajectory planning for assisting VANETs. Addressing connectivity disruptions in VANETs, a heterogeneous UAV-aided framework was proposed in [25] integrating a modified density-based clustering algorithm (MDBSCAN) and adaptive dual-model routing (ADMR). By employing a Multi-Agent Soft Actor-Critic approach for UAV trajectory optimization, this work significantly improved network reachability and data transmission performance. For UAV swarm-assisted Intelligent Transportation Systems, the work in [26] introduced over-the-air computation (AirComp) into edge services and proposed a DRL-based dual-scale intelligent AirComp (D2IAC) algorithm. This method jointly optimized UAV coordinates, service configuration, and power control, leading to substantial gains in coverage and resource efficiency.

However, the existing works of DRL-based connectivity enhancement in UAV-assisted VANETs faces several core challenges:

- Standard exploration strategies, such as ϵ -greedy or entropy regularization, are typically topology-agnostic, failing to incorporate semantic understanding of the road network. This deficiency leads to extremely slow training convergence or even failure to converge to an effective policy.
- DRL typically acquires all knowledge from scratch through trial-and-error learning. However, urban road networks inherently contain rich prior knowledge within their topological structures (e.g., *intersections are critical nodes for connectivity* or *arterial roads have high traffic density*). Traditional DRL methods struggle to directly leverage this structured semantic information, forcing UAVs to spend a vast number of episodes *rediscovering* the importance of intersections, thereby resulting in a massive waste of computational resources.
- Existing DRL-based solutions typically suffer from limited generalization capabilities when confronting significant variations in traffic patterns. Real-world urban traffic flows exhibit distinct characteristics in different time periods (e.g., the sharp contrast in vehicle density and distribution between rush hours and midnight). A policy trained on specific traffic scenarios often struggles to adapt to these unseen or drastically different flow distributions without extensive retraining, severely limiting

the practical applicability of DRL models in continuous, long-term UAV operations.

To address the aforementioned problems, we fine-tune an LLM to leverage the prior knowledge embedded in its vast knowledge base. By integrating this domain-specific topological expertise into the DRL agent’s learning process, we provide effective semantic guidance that transcends simple trial-and-error exploration. This approach not only accelerates convergence by avoiding blind exploration but also significantly enhances the agent’s generalization capability against dynamic shifts in urban traffic distributions.

3) *UAVs Controlled by LLM Agents*: In the domain of UAV control, several attempts have been made to utilize LLMs for high-level task planning or the translation of natural language instructions into control codes. For instance, to address GPS-denied indoor environments, a visual path planning method based on a fine-tuned LLM was proposed in [27]. By analyzing depth information and pedestrian location data, this approach generated flight trajectories with superior safety compared to traditional methods. Similarly, the study in [28] introduced a hybrid framework that utilized a Visual-Language Encoder (VLE) and a Retrieval-Augmented Generation (RAG)-empowered LLM to dynamically infer scene-specific safety margins, thereby guiding model predictive control (MPC) to achieve safe landings in dynamic environments. Furthermore, some studies employed LLMs to guide DRL training through reward shaping. Specifically, the LLM Enhanced Q-Learning Approach (LLM-QL) was developed in [29], which utilizes an LLM to generate heuristic reward terms, thereby guiding multi-UAV cooperative path exploration in complex, unknown environments. Targeting complex urban wind environments, the work in [30] proposed a hierarchical control architecture employing a fine-tuned LLM as a meta-decision maker. This system selected aggressive, balanced, or cautious Pareto-optimal RL flight policies in real-time based on building density and wind conditions.

However, existing LLM-guided UAV schemes typically suffer from two primary limitations:

- The LLM functioned solely as a high-level planner, generating coarse-grained waypoints, while low-level execution relied on traditional Proportional-Integral-Derivative (PID) controllers or simple path planning algorithms. This approach overlooked the subtle dynamic variations inherent in the low-level environment.
- While utilizing LLMs to generate auxiliary reward functions for guiding RL training is effective, designing appropriate prompts to yield stable numerical rewards is challenging and prone to introducing bias, potentially leading to *Reward Hacking* phenomena.

Consequently, we propose a deeper and more direct method of LLM integration. Specifically, we propose the Logit Fusion mechanism to intervene directly at the probability distribution level of action selection, thereby injecting the commonsense intuition of the LLM as a Prior Distribution into the Reinforcement Learning process.

B. Contributions

In response to the aforementioned challenges, we model the connectivity enhancement problem of UAV-aided VANETs as a dynamic dual graph connectivity maximization problem, thereby achieving a rigorous quantification of network connectivity metrics. Furthermore, we propose a novel four-stage architecture termed the Semantic-Augmented DRL (SA-DRL) Framework, in which LLMs are employed to interpret the complex urban environment, specifically extracting high-level road topological semantics that characterize the structural connectivity of the map. Building upon this foundation, we develop the Semantic-Augmented Proximal Policy Optimization (SA-PPO) algorithm, which incorporates the Logit Fusion mechanism to integrate these semantic priors, thereby explicitly guiding the agent’s action decision-making towards more effective deployment strategies. The main contributions of this paper are summarized as follows:

- We propose a graph-theoretic approach to rigorously quantify the fragmentation level of VANETs in complex urban environments. By constructing the Road Topology Graph (RTG) and the Dual Connectivity Graph (DCG), we reformulate the VANET fragmentation mitigation problem as a dynamic dual graph connectivity maximization problem, which exploits the UAV to merge disjoint vehicle clusters and maximize the average size of connected components.
- We design the **SA-DRL Framework**, which establishes a novel four-stage pipeline to bridge the gap between LLM reasoning and domain-specific control tasks. Through the integration of *Experience Collection*, *Semantic Prior Construction*, and *Knowledge Alignment*, this framework transforms a general-purpose LLM into a topology expert. Crucially, the framework leverages this aligned expert to actively guide the DRL agent’s exploration, thereby addressing the inefficiency of learning from scratch.
- We propose **SA-PPO**, a semantic-prior-augmented DRL algorithm that deeply integrates the fine-tuned LLM into the PPO decision-making loop. By employing a novel **Logit Fusion** mechanism, we directly inject the domain-specific expertise of the LLM as a semantic prior distribution into the policy generation process. This approach achieves a synergy between high-level expert reasoning and data-driven reinforcement learning, which significantly mitigates VANET fragmentation.
- We conduct extensive experiments on a high-fidelity simulator driven by real-world urban trajectories. Results demonstrate that SA-PPO outperforms state-of-the-art methods by improving key connectivity metrics by 13.2% and 23.5% while reducing energy consumption to 28.2%. Notably, it achieves these gains using only 26.6% of the training episodes, effectively mitigating mode collapse and blind exploration observed in traditional methods. Furthermore, the framework exhibits superior generalization among varying traffic distributions.

The remainder of this paper is organized as follows. Section II introduces the system model and formulates the optimization problem. Section III elaborates on the proposed SA-DRL

framework for addressing the optimization problem. Section IV presents the experimental results and discussions. Finally, Section V concludes this paper.

II. SYSTEM MODEL

A. Network Model

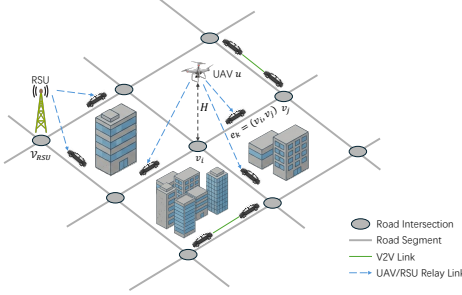


Fig. 1. UAV Aided VANET Scenario.

As illustrated in Fig. 1, we consider a UAV aided VANET system deployed within an urban region comprising n intersections and m road segments. The set of intersections within the task area is denoted as $\mathcal{I}_{road} = \{v_1, v_2, \dots, v_n\}$, while we represent the set of road segments as $\mathcal{S}_{road} = \{e_1, e_2, \dots, e_m\}$. Specifically, each intersection v_i possesses fixed 2D coordinates $\mathbf{p}_i = (x_i, y_i)$, and a road segment $e_k = (v_i, v_j)$ connects intersections v_i and v_j . Furthermore, a subset of intersections is equipped with fixed Roadside Units (RSUs), denoted as $\mathcal{V}_{RSU} \subset \mathcal{I}_{road}$. These intersections and their connecting segments maintain permanent network connectivity.

We assume that the operational timeline is discretized into a finite horizon of T time slots, denoted as $\mathcal{T} = \{1, 2, \dots, T\}$, where the duration of each slot is τ . In the time slot t , there are $N(t)$ vehicles traversing the road network. If a specific vehicle veh_l is located on the road segment e_k at the time slot t , its position is denoted as $pos_{veh,l} \in e_k$. While vehicle mobility follows the Intelligent Driver Model (IDM) [31], we assume that vehicle positions are known at the beginning of each time slot. Vehicles on the road establish connections with one another via onboard wireless interfaces, forming connected clusters. However, due to high vehicular mobility, intermittent connectivity gaps persist between these clusters, resulting in VANET fragmentation. Consequently, we consider the deployment of a UAV u as a communication relay to mitigate fragmentation and enhance network connectivity. The position of the UAV is denoted as $\mathbf{p}_u(t) = (x_u(t), y_u(t), H)$, where H represents a fixed flight altitude. Considering that urban structures (e.g., skyscrapers) can obstruct wireless signals, we assume that the UAV's flight destination in each time slot is positioned directly above a specific intersection $v \in \mathcal{I}_{road}$ to maximize the probability of establishing LoS connections with ground vehicles. It is worth noting that while we employ a single-UAV scenario for ease of discussion and implementation, our proposed method is equally applicable to multi-UAV scenarios and can be readily extended.

B. Communication Model

Given the specific characteristics of the urban environment, we adopt a probabilistic Air-to-Ground (A2G) channel model. The probability P_{LoS} of establishing a LoS link between the UAV and a ground node depends primarily on the elevation angle θ [32], which is expressed as

$$P_{LoS}(\theta) = \frac{1}{1 + a \cdot \exp(-b(\theta - a))}. \quad (1)$$

Here, $\theta = \frac{180}{\pi} \arctan\left(\frac{H}{d}\right)$ represents the elevation angle between the UAV and the ground vehicle, d is the horizontal Euclidean distance between the UAV and the ground vehicle, while a and b are S-curve parameters determined by the environment (e.g., dense urban, suburban, high-rise). The average path loss $L(d)$, modelled as the weighted sum of LoS and Non-Line-of-Sight (NLoS) losses, is given by

$$L(d) = P_{LoS} \cdot L_{LoS}(d) + (1 - P_{LoS}) \cdot L_{NLoS}(d), \quad (2)$$

where L_{LoS} and L_{NLoS} represent the free-space path loss plus additional attenuation loss in the two respective states, expressed as

$$L_{\xi}(d) = 20 \log\left(\frac{4\pi df_c}{c}\right) + \eta_{\xi}, \quad \xi \in \{LoS, NLoS\}. \quad (3)$$

Here, f_c is the carrier frequency, c is the speed of light, while η_{LoS} and η_{NLoS} denote the average additional losses (shading loss) under LoS and NLoS conditions, respectively. Let P_{tx} be the UAV transmission power, and G be the sum of the receiver and transmitter antenna gains. The signal power received by a ground vehicle is given by

$$P_{rx}(d) = P_{tx} + G - L(d). \quad (4)$$

The maximum distance d satisfying $P_{rx}(d) \geq P_{th}$ is defined as the UAV coverage radius R_{cov} , where P_{th} is the minimum received power required to satisfy Quality of Service (QoS) requirements. We assume that if a UAV is positioned directly above intersection v , and its wireless coverage radius R_{cov} exceeds half the length of the road segment, the UAV is capable of covering all vehicles situated on the road segments incident to intersection v . Furthermore, we assume that the communication range of the UAV under unobstructed conditions is sufficient to cover half the length of any road segment, thereby ensuring that vehicles located on the same road segment can be interconnected through multi-hop transmission.

C. Graph-Theoretic Model of VANET Fragmentation

Definition 1 (Road Topology Graph (RTG)): An undirected weighted graph $\mathcal{G} = (\mathcal{V}, \mathcal{E})$ is defined as the RTG corresponding to the urban road network $(\mathcal{I}_{road}, \mathcal{S}_{road})$, if there exist bijections $\phi: \mathcal{I}_{road} \rightarrow \mathcal{V}$ and $\psi: \mathcal{S}_{road} \rightarrow \mathcal{E}$, such that for $\forall s = (i_1, i_2) \in \mathcal{I}_{road}$, the condition $\psi(s) = (\phi(i_1), \phi(i_2))$ holds. Meanwhile, the weight of a vertex $v \in \mathcal{V}$ is defined as

$$p_v(t) = \begin{cases} 0, & \text{if } \phi^{-1}(v) \text{ is currently not covered,} \\ 1, & \text{if } \phi^{-1}(v) \text{ is covered by an RSU,} \\ 2, & \text{if UAV } u \text{ is located at } \phi^{-1}(v). \end{cases} \quad (5)$$

In particular, when the UAV u is positioned at an intersection covered by an RSU, we define $p_v(t) = 2$. The weight of an edge $e \in \mathcal{E}$ is defined as

$$p_e(t) = \text{NumVehicles}(e, t), \quad (6)$$

which represents the total number of vehicles located on the road segment e during the time slot t .

The vertex weights of the RTG characterize the coverage status of intersections, while the edge weights describe the traffic load on urban roads. To facilitate optimization in large-scale networks, we define *c-edge* and *c-vertex* as follows to characterize the connectivity of RTG vertices and edges. This allows us to abstract the complex determination of VANET connectivity into a graph-theoretic coverage problem.

Definition 2 (Connected Vertex (c-vertex)): Consider a vertex $v \in \mathcal{V}$, v is designated as a *c-vertex* in time slot t if and only if at least one of the following conditions is met:

- 1) $p_v(t) \geq 0$;
- 2) $\exists e \in \delta(v), p_e(t) > 0$.

Here, $\delta(v)$ denotes the set of edges incident to vertex v .

Definition 3 (Connected Edge (c-edge)): Consider an edge $e = (v_1, v_2) \in \mathcal{E}$, e is designated as a *c-edge* in time slot t if and only if at least one of the following conditions is met:

- 1) $p_e(t) > 0$;
- 2) v_1 or v_2 is a *c-vertex*.

Building upon the concepts of *c-edge* and *c-vertex*, we define the *c-graph* as follows.

Definition 4 (Connected Graph (c-graph)): Let $\mathcal{V}_c(t)$ and $\mathcal{E}_c(t)$ denote the sets of all *c-vertices* and *c-edges* in the RTG \mathcal{G} at the time slot t , respectively. We define the *c-graph* as the subgraph $\mathcal{G}_c(t) = (\mathcal{V}'(t), \mathcal{E}'(t))$, where the edge set is given by $\mathcal{E}'(t) = \mathcal{E}_c(t)$, and the vertex set $\mathcal{V}'(t)$ is composed of $\mathcal{V}_c(t)$ and its associated edge endpoints, i.e.

$$\mathcal{V}'(t) = \mathcal{V}_c(t) \cup \{v \in \mathcal{V} \mid \exists e \in \mathcal{E}_c(t), v \in e\}. \quad (7)$$

Since vehicles in VANETs are primarily located on road segments rather than at intersections, the connected components of \mathcal{G}_c are insufficient to accurately quantify the degree of VANET fragmentation. This is because connected components are typically based on vertex reachability, whereas VANET connectivity should fundamentally be regarded as a form of Edge-based Connectivity. Consequently, we employ a dual graph approach by considering the following definition.

Definition 5 (Dual Connected Graph (DCG)): Consider the *c-graph* $\mathcal{G}_c(t) = (\mathcal{V}'(t), \mathcal{E}'(t))$, for $\forall e \in \mathcal{E}'(t)$, based on a bijection $\varphi : \mathcal{E}'(t) \rightarrow \mathcal{V}^*(t)$, we define a unique vertex $v^* = \varphi(e) \in \mathcal{V}^*(t)$. For $\forall v \in \mathcal{V}'(t)$ and any two incident edges $e_1, e_2 \in \delta(v)$, we define an edge $(\varphi(e_1), \varphi(e_2)) \in \mathcal{E}^*(t)$. The undirected weighted graph $\mathcal{G}^*(t) = (\mathcal{V}^*(t), \mathcal{E}^*(t))$ is termed the *DCG* corresponding to $\mathcal{G}_c(t)$. For any $v^* \in \mathcal{V}^*(t)$, its weight is defined as the weight of the corresponding edge in the primal graph, which can be expressed as

$$p_{v^*}(t) = p_{\varphi^{-1}(v^*)}(t). \quad (8)$$

The connected subnets (i.e., network fragments) of the VANET exhibit a one-to-one correspondence with the connected components in the DCG. Moreover, the number of

vehicles within a connected subnet is equivalent to the sum of the vertex weights of the corresponding connected components. Consequently, we quantify the degree of VANET fragmentation utilizing the connected components of the DCG. Let $K(t)$ denote the number of connected components in $\mathcal{G}^*(t)$, with the corresponding sums of vertex weights denoted as $n_1(t), \dots, n_{K(t)}(t)$, we define

$$C(t) = \frac{1}{K(t)} \sum_{i=1}^{K(t)} n_i(t). \quad (9)$$

Here, $K(t)$ represents the number of VANET network fragments, while $C(t)$ signifies the average number of vehicles within each fragment. Consequently, a smaller $K(t)$ and a larger $C(t)$ indicate the better network connectivity.

D. Energy Consumption Model

We model the energy consumption of UAV u in time slot t as the sum of propulsion energy $e_f(t)$, hovering energy $e_h(t)$, and communication energy $e_c(t)$. To ensure reliable communication quality and mitigate Doppler shifts caused by UAV mobility, we adopt the hover-and-transmit paradigm [33]. Similar to the approach in [34], we assume a constant flight velocity for the UAV. Thus, $e_f(t)$ is proportional to the flight distance, while $e_h(t)$ and $e_c(t)$ are proportional to the hovering duration. Suppose the UAV flies from intersection v_i to intersection v_j in time slot t with velocity v_u , the total energy consumption in time slot t is given by

$$\begin{aligned} E(t) &= e_f(t) + e_h(t) + e_c(t) \\ &= (\varepsilon_1 + \varepsilon_2) \left(\tau - \frac{l(v_i, v_j)}{v_u} \right) + \varepsilon_3 \cdot \frac{l(v_i, v_j)}{v_u}. \end{aligned} \quad (10)$$

Here, $l(v_i, v_j)$ represents the Euclidean distance between the two intersections, while $\varepsilon_1, \varepsilon_2$, and ε_3 denote the power consumption for hovering, communication, and propulsion, respectively.

E. Problem Formulation

To simultaneously minimize VANET fragmentation and UAV energy consumption, we formulate the dynamic deployment problem for the UAV-assisted VANET as

$$\max_{\mathbf{P}_u} \sum_{t=1}^T (C(t) - E(t)) \quad (11)$$

$$\text{s.t. } \mathbf{p}_u(t) \in \mathcal{I}_{road}, t \in [1, T] \quad (11a)$$

$$l(\mathbf{p}_v(t-1), \mathbf{p}_v(t)) \leq v_u \tau, t \in [1, T] \quad (11b)$$

$$E_{battery} - \sum_{t=1}^T E(t) > 0 \quad (11c)$$

where $\mathbf{P}_u = \{\mathbf{p}_u(1), \dots, \mathbf{p}_u(T)\}$ represents the sequence of UAV positions at all time slots, and $E_{battery}$ is the UAV battery capacity. Constraint (11a) requires that the UAV's target destination in each time slot is an intersection. Constraint (11b) ensures that the flight distance in each time slot does not exceed the maximum distance feasible under the velocity limit. Constraint (11c) mandates that the UAV's

energy is not depleted before the mission concludes. The above problem represents a typical Mixed-Integer Non-Linear Programming (MINLP) problem. Due to the stochastic nature of the vehicular distribution $p_e(t)$ and the vastness of the state space, where the number of trajectory combinations grows exponentially with the number of intersections n , traditional optimization methods are computationally intractable. This challenge motivates the introduction of DRL in this study.

III. PROPOSED APPROACH

To address the aforementioned challenges, we propose a novel LLM-guided DRL framework, termed *Semantic-Augmented Deep Reinforcement Learning* (SA-DRL), to solve the optimization problem formulated in (11). As illustrated in Fig. 2, the SA-DRL framework operates via a four-stage pipeline. Specifically, we gather experience through environmental exploration, extract semantics from this experience to construct datasets, and achieve knowledge alignment of the pre-trained LLM regarding the specific topology of urban networks via Parameter-Efficient Fine-Tuning (PEFT). Moreover, we propose the *Semantic-Augmented Proximal Policy Optimization* (SA-PPO) algorithm, which integrates the semantic reasoning capabilities of the LLM into the decision-making loop of the DRL agent through a Logit Fusion mechanism. This joint architecture effectively mitigates the challenges associated with blind exploration and the deficiency in topological understanding inherent in traditional DRL.

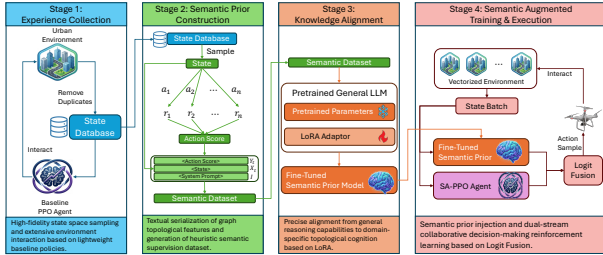


Fig. 2. The four-stage pipeline of the SA-DRL framework.

In the following, we first introduce the key elements of DRL. Subsequently, we elaborate on the specific details of each stage within the pipeline. Finally, we summarize the proposed SA-DRL framework.

A. Key Elements of DRL

We model the dynamic UAV deployment task as a Markov Decision Process (MDP) to solve the optimization problem formulated in (11) using DRL algorithms. An MDP is defined by the tuple $(\mathcal{S}, \mathcal{A}, r, \gamma)$, representing the state space, action space, reward function, and discount factor.

1) *Action Space*: We constrain the UAV's flight destination to always be an intersection. Therefore, $\mathcal{A} = \mathcal{V}$, and the size of the agent's action space is n .

2) *State Space*: We define the state at time slot t as

$$s(t) = \{p_e(t)|e \in \mathcal{E}\} \cup \{p_v(t)|v \in \mathcal{V}\}. \quad (12)$$

When used as input for the DRL algorithm, $s(t)$ requires normalization.

3) *Reward Function*: We define the agent's reward at time slot t as

$$r(t) = \alpha \cdot \frac{1}{K(t)} - \beta \cdot \frac{E(t)}{E_0}, \quad (13)$$

where α and β are weighting coefficients, and E_0 represents the maximum energy consumption of the UAV per time slot.

B. Stage 1: Experience Collection

Algorithm 1: Experience Collection

Input: Target number N_{target} , maximum number of training episodes K_{max} .
Output: State database \mathcal{D}_{State} .

- 1 Initialize empty database $\mathcal{D}_{State} \leftarrow \emptyset$;
- 2 Initialize baseline PPO policy π_θ with random weights;
- 3 Initialize PPO replay buffer \mathcal{B} ;
- 4 **for** $k \leftarrow 1$ **to** K_{max} **do**
- 5 Reset environment and observe initial state s_0 ;
- 6 **for** $t = 1$ **to** T **do**
- 7 Select action $a_t \sim \pi_\theta(\cdot|s_t)$;
- 8 Execute action a_t , observe reward r_t and next state s_{t+1} ;
- 9 **if** $s_t \notin \mathcal{D}_{State}$ **then**
- 10 $\mathcal{D}_{State} \leftarrow \mathcal{D}_{State} \cup \{s_t\}$;
- 11 **if** $|\mathcal{D}_{State}| \geq N_{target}$ **then**
- 12 **return** \mathcal{D}_{State}
- 13 **end**
- 14 **end**
- 15 Store transition (s_t, a_t, r_t, s_{t+1}) in \mathcal{B} ;
- 16 $s_t \leftarrow s_{t+1}$;
- 17 **end**
- 18 **if** *update condition met* **then**
- 19 Update π_θ using data in \mathcal{B} via standard PPO loss;
- 20 Clear \mathcal{B} ;
- 21 **end**
- 22 **end**
- 23 **return** \mathcal{D}_{State}

As outlined in Algorithm 1, in this stage, we collect states that the agent may encounter during operation through simple environmental exploration and store them in a state database \mathcal{D}_{state} . Specifically, we train a lightweight baseline PPO agent to explore the environment briefly and collect states encountered during the rollout process, which are then added to the database after deduplication. Compared to random walk sampling, the states collected by a lightweight DRL baseline are closer to the real task distribution. This approach enhances dataset quality, thereby improving training efficiency during LLM fine-tuning.

C. Stage 2: Semantic Prior Construction

As shown in Algorithm 2, in this stage, we transform numerical graph states into semantic tokens processable by the LLM and construct a Supervised Fine-Tuning (SFT) dataset based on the state database \mathcal{D}_{state} . Considering that directly

Algorithm 2: Semantic Prior Construction

Input: State database \mathcal{D}_{state} , system prompt I_{task} .

Output: SFT dataset \mathcal{D}_{sft} .

```

1 Initialize empty dataset  $\mathcal{D}_{sft} \leftarrow \emptyset$ ;
2 foreach  $s$  in  $\mathcal{D}_{state}$  do
3   Initialize reward vector  $\mathbf{r} \leftarrow \text{zeros}(n)$ ;
4   foreach  $a$  in  $\mathcal{A}$  do
5     Restore environment to state  $s$ ;
6     Execute action  $a$  and observe immediate
       reward  $r_a$ ;
7      $\mathbf{r}[a] \leftarrow r_a$ ;
8   end
9   Compute discrete action scores  $Y_t$  from  $\mathbf{r}$  using
     Eq. (14);
10   $X_t \leftarrow \text{Serialize}(s)$ ;
11   $D_t \leftarrow \{\text{"instruction"} : I, \text{"input"} : X_t, \text{"output"} :
     Y_t\}$ ;
12   $\mathcal{D}_{sft} \leftarrow \mathcal{D}_{sft} \cup \{D_t\}$ ;
13 end
14 return  $\mathcal{D}_{sft}$ 

```

inputting the graph adjacency matrix into the LLM is inefficient, we propose a concise serialization method to capture key topological features. To capture the semantic essence of VANET fragmentation, we transform the numerical state s_t into a textual description of the connectivity landscape. Specifically, *vehicle_per_edge* does not merely count cars but semantically represents traffic density hotspots that require coverage, while *node_weight* identifies backhaul-enabled intersections, which allows the LLM to perceive the road network not as a matrix, but as a set of disconnected vehicular clusters waiting to be bridged.

To transform the LLM into a domain expert, we construct an instruction fine-tuning dataset $\mathcal{D}_{sft} = \{(I, X_t, Y_t)\}$. Here, I is the system prompt guiding the task, informing the LLM of basic task information; X_t is the serialized s_t , and Y_t represents the output **action score**. Since directly computing the optimal state-value function $Q^*(s_t, \cdot)$ is intractable, we employ the immediate reward $r(s_t, \cdot)$ as an approximate action score. Although the immediate reward is myopic, it serves as a robust indicator of topological criticality within the dynamic network. A high score signifies an intersection capable of healing partitions in the DCG or merging disjoint vehicle platoons. Through SFT on this dataset, the LLM learns the mapping $f_{LLM} : X_t \rightarrow P_{prior}(a|s)$, thereby providing a commonsense distribution over the action space. It is important to note that floating-point data not only consume more tokens but also increase the learning difficulty for the LLM. Therefore, the state vectors fed into the LLM must utilize integer components and strictly avoid normalization. Since the immediate reward defined in (13) is presented in floating-point format, we map it from the continuous interval $(-1, 1)$ to the discrete interval $[0, score^*] \cap \mathbb{Z}$ via (14). In practical implementation, to ensure a fixed output length for the LLM, $score^*$ is set to 9, ensuring that each component of Y_t occupies only a single character.

Thus, we have

$$Y_t = \text{round} \left(\frac{r(s_t, \cdot) - \min r(s_t, \cdot)}{\max r(s_t, \cdot) - \min r(s_t, \cdot)} \cdot score^* \right). \quad (14)$$

D. Stage 3: Knowledge Alignment

Although pre-trained LLMs possess extensive common-sense knowledge, they lack physical intuition regarding urban mobility and propagation constraints. General LLMs do not inherently understand that vehicles are confined to road geometries or that specific intersections act as LoS bottlenecks due to urban canyons. Moreover, without fine-tuning, LLMs struggle to consistently generate structured outputs (e.g., in JSON format). Current solutions primarily rely on designing rigorous prompts or employing SFT. However, the former imposes high demands on the model’s intrinsic capabilities, making it difficult to implement on smaller models. Moreover, the study in [35] indicates that such strict prompting strategies may compromise the LLM’s performance. Given the substantial inference demands associated with utilizing LLMs to guide DRL training, we adopt Low-Rank Adaptation (LoRA) [36] for knowledge alignment. This approach enables the adaptation of the LLM to the action scoring task without incurring the prohibitive computational costs of full-parameter training. As shown in Fig. 3, LoRA freezes the pre-trained backbone weights \mathbf{W} and injects trainable low-rank adapter matrices \mathbf{A} and \mathbf{B} into the linear layers. The forward pass is approximated as

$$\mathbf{Y} = \mathbf{X}(\mathbf{W} + \Delta\mathbf{W}) = \mathbf{X}(\mathbf{W} + \mathbf{B}\mathbf{A}), \quad (15)$$

where \mathbf{B} and \mathbf{A} are matrices of rank r , with r being significantly smaller than the original model dimension. By optimizing \mathbf{A} and \mathbf{B} exclusively on \mathcal{D}_{sft} , the model aligns its probability distribution with the topological requirements of the urban grid while preserving its inherent reasoning capabilities. Furthermore, this ensures that the model’s output consistently adheres to a strict JSON format.

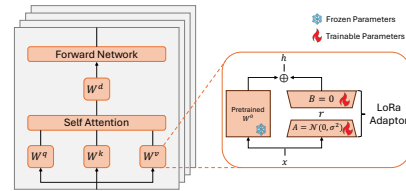


Fig. 3. Schematic diagram of the LoRA fine-tuning mechanism.

E. Stage 4: Semantic-Augmented Training & Execution

In this stage, we proceed to train the final SA-PPO agent. As illustrated in Fig. 4, to mitigate the issue of blind exploration inherent in traditional DRL, we deeply integrate the semantic priors derived from the fine-tuned LLM with the PPO policy network via a Logit Fusion mechanism. Furthermore, we employ an objective function incorporating KL regularization to guide the agent’s exploration within the semantic space. Benefiting from the robust semantic understanding capabilities and the extensive pre-trained knowledge base of LLMs, the incorporation of semantic priors enhances the algorithm’s generalization ability and simultaneously improves training efficiency.

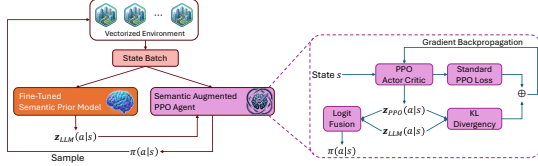


Fig. 4. Schematic diagram of the SA-PPO training and execution mechanism.

1) *Dual-Stream Inference and Logit Fusion*: To combine semantic priors with real-time control policies, we design a dual-stream inference architecture. The PPO Actor network receives the state vector s_t and outputs the raw logits vector z_{PPO} over the action space via a Multilayer Perceptron (MLP), i.e.

$$z_{PPO} = \text{MLP}_{actor}(s_t). \quad (16)$$

Simultaneously, we serialize the current state into a text token sequence X_t and obtain the semantic prior Y_t outputted by the fine-tuned LLM. This is then normalized to serve as the raw logits vector output by the LLM, i.e.

$$z_{LLM} = \frac{Y_t - \mu(Y_t)}{\sigma(Y_t) + \varepsilon}. \quad (17)$$

Here, μ is the mean, σ denotes the standard deviation, and $\varepsilon = 10^{-7}$ represents a small positive constant. The final execution policy $\tilde{\pi}$ is generated by the weighted fusion of these two logits followed by Softmax activation. We term this step **Logit Fusion**, which establishes a hierarchical control synergy. The LLM acts globally, analyzing the RTG to recommend bridge nodes essential for network integrity. Simultaneously, the PPO agent functions acts locally, refining these recommendations based on real-time feedback to handle transient vehicle fluctuations. This fusion ensures the UAV executes a semantic-aware deployment, anchoring to critical hubs while adaptively maneuvering for optimal signal coverage, which is given by

$$\tilde{\pi}(\cdot|s_t) = \frac{\exp(z_{PPO} + \lambda \cdot z_{LLM})}{\sum_{j=1}^n \exp(z_{PPO}^{(j)} + \lambda \cdot z_{LLM}^{(j)})}. \quad (18)$$

2) *Objective Function with KL Regularization*: To enable the LLM's commonsense recommendations to effectively guide PPO learning, we introduce a KL divergence regularization term into the standard PPO loss function. The total loss function $L(\theta)$ for SA-PPO is defined as

$$L = \mathbb{E}_t[-L_t^{CLIP} + c_1 L_t^{VF} - c_2 S[\tilde{\pi}](s_t) + \beta D_{KL}(\tilde{\pi}(\cdot|s_t) || \pi_{LLM}(\cdot|X_t))], \quad (19)$$

where L_t^{CLIP} is the PPO clipped surrogate objective, L_t^{VF} denotes the PPO value function loss, $S[\tilde{\pi}](s_t)$ represents the PPO entropy regularization, and D_{KL} is the KL divergence. The KL term constrains the PPO policy distribution from deviating excessively from the semantic prior π_{LLM} provided by the LLM, thereby acting as a guardrail to guide the agent's exploration within a valid semantic space, which effectively improves the training efficiency of the algorithm. Finally, the training and execution procedure of SA-PPO is outlined in Algorithm 3.

Algorithm 3: Semantic-Augmented Training & Execution of SA-PPO

Input: Fine-tuned LLM \mathcal{M}_{SFT} , maximum number of training episodes K_{max} .

- 1 Initialize S2A-PPO agent \mathcal{M}_θ with random weights θ ;
 - 2 Initialize replay buffer \mathcal{B} ;
 - 3 **for** $k \leftarrow 1$ **to** K_{max} **do**
 - 4 Reset environment;
 - 5 **for** $t = 1$ **to** T **do**
 - 6 Observe current state s_t ;
 - 7 $X_t \leftarrow \text{Serialize}(s_t)$;
 - 8 $z_{LLM} \leftarrow \mathcal{M}_{SFT}(I, X_t)$;
 - 9 $z_{PPO} \leftarrow \mathcal{M}_\theta(s_t)$;
 - 10 Get $\tilde{\pi}(\cdot|s_t)$ with Eq. (18);
 - 11 Select action $a_t \sim \tilde{\pi}(\cdot|s_t)$;
 - 12 Execute action a_t , observe reward r_t and next state s_{t+1} ;
 - 13 Store transition $(s_t, a_t, r_t, s_{t+1}, z_{LLM}, z_{PPO})$ in \mathcal{B} ;
 - 14 **end**
 - 15 **if** *update condition met* **then**
 - 16 Update π_θ using data in \mathcal{B} with Eq. (19);
 - 17 Clear \mathcal{B} ;
 - 18 **end**
 - 19 **end**
-

F. High-Throughput Parallel Training System

A major bottleneck in LLM-assisted DRL is inference latency. Considering that existing LLM inference engines can significantly increase inference speed when handling batch tasks (as opposed to serial execution), we implement a vectorized parallel training system. Instead of using a single thread for interaction sampling, we generate N parallel environments to simultaneously collect a batch of states $S_{batch} = \{s_1, \dots, s_N\}$. These states are serialized and inputted into the LLM inference engine as a batch. This mechanism renders On-Policy training utilizing LLM priors computationally feasible in large-scale urban scenarios.

G. SA-DRL Framework

Algorithm 4 outlines the execution workflow of the SA-DRL framework. First, a lightweight exploration phase (Algorithm 1) is executed utilizing the pre-trained model \mathcal{M}_{base} to construct a database \mathcal{D}_{State} encompassing diverse states. Subsequently, a high-quality supervised fine-tuning dataset \mathcal{D}_{sft} is constructed via state serialization and action scoring (Algorithm 2). Building upon this, LoRA adapters are introduced to fine-tune \mathcal{M}_{base} , yielding an intermediate model \mathcal{M}_{SFT} equipped with domain-specific semantic priors. Finally, the SA-PPO agent \mathcal{M}_θ is initialized to perform online reinforcement learning under the semantic guidance provided by \mathcal{M}_{SFT} (Algorithm 3), ultimately resulting in a converged policy model.

Algorithm 4: The SA-DRL Framework

Input: Pre-trained LLM \mathcal{M}_{base} , System Prompt I_{task} , K_{max} , N_{target} .

Output: Optimized SA-PPO agent \mathcal{M}_θ .

- 1 Execute lightweight exploration to collect state database \mathcal{D}_{State} via **Algorithm 1**;
 - 2 Serialize states and compute action scores to construct SFT dataset \mathcal{D}_{sft} via **Algorithm 2**;
 - 3 Initialize LoRA adapters for \mathcal{M}_{base} ;
 - 4 Fine-tune \mathcal{M}_{base} on \mathcal{D}_{sft} to obtain the domain-specific semantic model \mathcal{M}_{SFT} ;
 - 5 Initialize SA-PPO agent \mathcal{M}_θ ;
 - 6 Train \mathcal{M}_θ online guided by semantic priors from \mathcal{M}_{SFT} via **Algorithm 3**;
 - 7 **return** *Converged SA-PPO agent* \mathcal{M}_θ
-

IV. PERFORMANCE EVALUATION

A. System Setup

We utilize the dataset from [37], which provides topological urban maps and vehicle trajectories collected by large-scale traffic surveillance systems in two Chinese cities. The original dataset contains approximately 5 million records over four days. To speed up simulations, we generate a small-scale subset based on the data for a specific area in Shenzhen on April 16, 2021, consisting of 47 nodes, 88 edges, and 5,000 trajectory records. Based on this data set, we construct a Python simulation system to implement the four-stage SA-DRL pipeline. Figure 5 depicts the RTG of the simulated network, where the red node marks the UAV’s starting position (Node 9), green nodes denote intersections equipped with RSUs (Nodes 11-13), and blue nodes represent standard road intersections. Following this setup, we conduct comparative experiments and ablation studies to verify the algorithm’s effectiveness. In terms of implementation, we use PyTorch for the SA-PPO algorithm, LLaMA Factory [38] for LLM fine-tuning, and the vLLM [39] framework for inference acceleration. The experimental hardware consists of an Intel Core i7-14700KF @ 3.42 GHz CPU and an NVIDIA GeForce RTX 4080 Super GPU.

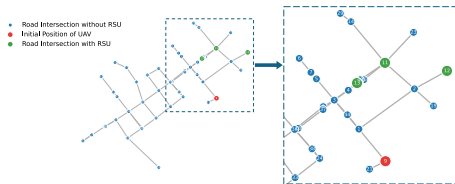


Fig. 5. The RTG corresponding to the road network used in simulation.

B. Analysis of the Semantic Prior Model

1) *Performance Evaluation of Semantic Knowledge Alignment:* In addition to standard LLM evaluation metrics such as the Bilingual Evaluation Understudy (Cumulative 4-gram score, BLEU-4) and the Recall-Oriented Understudy for Gisting Evaluation (based on Longest Common Subsequence, ROUGE-L), we introduce three specific evaluation metrics tailored to the algorithm’s characteristics:

- **JSON Parsing Success Rate (JSON PSR):** Given that the DRL training loop requires automated interaction, the LLM output must strictly adhere to the defined JSON schema. We define the JSON Parsing Success Rate as the proportion of generated responses that can be successfully decoded by a standard JSON parser without syntax errors (e.g., missing brackets, unescaped characters). We have

$$PSR = \frac{1}{N} \sum_{i=1}^N \mathbb{I}(\text{isValidJSON}(o_i)). \quad (20)$$

- **Kendall’s Rank Correlation Coefficient (Kendall’s τ):** This metric quantifies the ordinal association between the semantic scores predicted by the LLM and the ground-truth heuristic rewards. Unlike absolute value-based metrics (e.g., Mean Squared Error), Kendall’s τ focuses on the relative ranking of candidates, which is crucial for DRL agents that select actions based on relative dominance. Given two sequences of equal length \mathbf{x}, \mathbf{y} , we enumerate all pairs of positions (i, j) . When $(x_i - x_j)(y_i - y_j) > 0$ (concordant pairs), we let the count be C . As for $(x_i - x_j)(y_i - y_j) < 0$ (discordant pairs), we let the count be D . Then, Kendall’s τ is defined as

$$\tau = \frac{C - D}{C + D}. \quad (21)$$

A larger τ indicates a higher correlation in ranking between the two sequences. $\tau = 1$ implies identical ranking, while $\tau = -1$ implies completely opposite ranking.

- **Top- k Hit Rate (HR_k):** Beyond global ranking correlation, a critical metric is ensuring that optimal actions are included within the high-probability candidate set. We adopt a set-based Top- k Hit Rate. Specifically, for each state, we sort both the predicted semantic scores and the ground-truth heuristic rewards in descending order to extract two index subsets: the top- k predicted set $\mathcal{S}_{pred}^{(k)}$ and the top- k ground truth set $\mathcal{S}_{gt}^{(k)}$. To calculate the ratio of the cardinality of their intersection, we define

$$HR_k = \frac{1}{M} \sum_{i=1}^M \frac{|\mathcal{S}_{pred,i}^{(k)} \cap \mathcal{S}_{gt,i}^{(k)}|}{k}, \quad (22)$$

where M is the number of samples. This metric quantifies the overlap ratio, indicating the accuracy with which the LLM captures the set of dominant topological nodes. In the subsequent presentation of results, we set $k = 10$.

To evaluate the impact of different backbone architectures on topological reasoning and instruction-following capabilities, we benchmark four state-of-the-art lightweight LLMs: Qwen2.5-3B, Qwen3-4B, Llama3.2-3B, and Gemma3-4B. We focus on models with less parameters to ensure the feasibility of deployment on resource-constrained UAVs. The comparative results are summarized in Table I.

As demonstrated in the first two columns of Table I, the necessity of the knowledge alignment phase (Stage 3) is undeniable. The base model (without SFT) exhibits a complete failure in the instruction-following task, yielding a JSON PSR

TABLE I
PERFORMANCE EVALUATION OF SEMANTIC KNOWLEDGE ALIGNMENT

LLM	Qwen3	Qwen3	Qwen2.5	Llama3.2	Gemma3
Parameters	4B	4B	3B	3B	4B
SFT	None	LoRA	LoRA	LoRA	LoRA
BLEU-4	0.20	<u>70.32</u>	74.32	44.64	55.50
ROUGE-L	7.78	<u>78.42</u>	81.68	69.81	74.84
Kendall's τ	nan	<u>78.82</u>	85.03	<u>85.60</u>	88.89
JSON PSR	0.00	100.00	100.00	100.00	100.00
HR_{10}	0.00	51.11	<u>56.60</u>	55.53	58.60

of 0.00% and a BLEU score approaching zero. This indicates that without domain-specific fine-tuning, general-purpose LLMs are incapable of generating valid JSON structures or comprehending action scoring logic. In contrast, after applying LoRA fine-tuning (Qwen3-4B), the success rate surges to 100%, and the topological reasoning capability is significantly enhanced, achieving a Kendall's τ of 78.82. This validates that our parameter-efficient fine-tuning strategy successfully transforms the LLM from a generic chatbot into a well-trained topology expert. However, notable performance disparities are observed among the fine-tuned models. While Gemma3-4B achieves marginally superior topological ranking accuracy, Qwen2.5-3B demonstrates enhanced performance in terms of textual consistency. This trade-off between precision and potential computational cost necessitates a further evaluation incorporating inference efficiency to determine the final model selection.

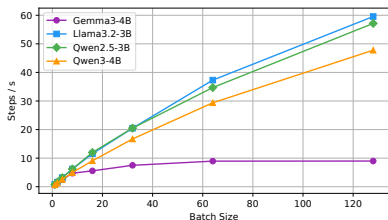


Fig. 6. Inference efficiency comparison for different LLM architectures as batch size varies.

2) *Inference Efficiency Analysis*: While semantic alignment is imperative, the inherent high-frequency interaction characteristic of DRL imposes stringent constraints on inference latency. Although our proposed parallel training system enables batch inference, the scalability of the underlying LLM remains a critical bottleneck determining the overall training efficiency. As illustrated in Fig. 6, we observe a critical performance divergence as the batch size increases. The throughput of Gemma3-4B (purple line) saturates rapidly, stagnating at approximately 9 steps/s regardless of the increase in batch size. This indicates a severe VRAM bottleneck (e.g. the VRAM available for the KV-Cache is insufficient), likely attributable to its larger parameter count and architectural overhead, rendering it unsuitable for parallelized training environments. In contrast, Qwen2.5-3B (green line) demonstrates superior scalability. Its throughput exhibits a linear increase with batch size, peaking at approximately 58 steps/s at a batch size of 128, which is more than 6 times faster than Gemma3-4B. This high-throughput capability enables the SA-PPO agent to collect samples and update its policy significantly faster, thereby substantially reducing the total training duration. In

summary, although Gemma3-4B holds a marginal advantage in semantic reasoning, its suboptimal inference efficiency imposes an unacceptable computational burden on the system. Consequently, we select Qwen2.5-3B as the backbone network and set the batch size to 128, thereby striking an optimal balance between reasoning capability and system efficiency.

3) *Visual Analysis of Semantic Alignment*: To provide a more intuitive understanding of the efficacy of semantic alignment, we visualize the action score distributions generated by the LLMs. Fig. 7 presents a heatmap comparison between the average semantic scores predicted by different fine-tuned models and the ground truth (Label) on the test set. In this visualization, the x-axis represents the index of intersection nodes (Action Index), while the color intensity corresponds to the average action score. Variations in color distribution reflect the differing learning capabilities of the models regarding the environment. However, the overall trends reveal the intrinsic topological characteristics of the urban landscape. Since the heatmap represents aggregated scores across all test states, the vertical bands consistently exhibiting high scores (e.g., Nodes 34 and 10) identify nodes possessing high global centrality or strategic importance. By cross-referencing with the road topology map in Fig. 5, we observe that these high-scoring indices correspond to critical traffic hubs (notably, they are all cut vertices of the graph). This correspondence confirms that the fine-tuned LLMs have successfully internalized the spatial structure of the road network, learning to prioritize topologically critical nodes while abstracting away transient traffic fluctuations.

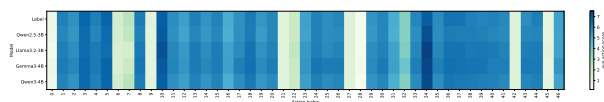


Fig. 7. Heatmap comparison of action scores predicted by different fine-tuned LLMs against ground truth.

Furthermore, to validate the stability of the selected backbone model, Fig. 8 details the prediction performance of Qwen2.5-3B across multiple random samples. The upper row displays the ground truth labels, while the lower row shows the model predictions. The results indicate that the model successfully generalizes across diverse topological states, consistently identifying key intersections and reproducing the sparse distribution characteristics of the reward function. This confirms that the LoRA-based fine-tuning has successfully aligned the reasoning capabilities of the LLM with the domain-specific requirements of urban vehicular networks.

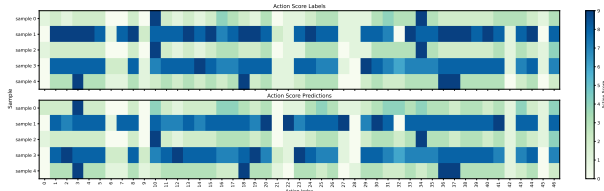


Fig. 8. Comparison of action score predictions by Qwen2.5-3B against ground truth.

C. Performance Evaluation of SA-PPO

1) *Comparative Experiments*: To validate the effectiveness of the proposed SA-PPO algorithm in dynamic UAV deployment, we compare it against three representative DRL baselines. These baselines encompass standard On-Policy and Off-Policy algorithms, as well as graph-reinforced DRL methods.

- **Soft Actor-Critic (SAC)**: An Off-Policy DRL algorithm utilized in [40] to optimize the Age of Information (AoI) in UAV-aided vehicular edge computing. SAC enhances exploration by simultaneously maximizing reward and policy entropy.
- **Vanilla PPO** [13]: The standard Proximal Policy Optimization algorithm (On-Policy) without any semantic or structural enhancements. The agent observes raw state vectors and learns solely through trial-and-error interactions with the environment.
- **GAT-PPO**: A PPO variant that employs a Graph Attention Network (GAT) as the feature extractor, replacing the standard Multi-Layer Perceptron (MLP). Since our environment is modeled based on RTG, GAT-PPO is designed to explicitly extract structured data from the graph.
- **SA-PPO (Ours)**: The proposed algorithm which integrates the domain-specific topological expertise of a fine-tuned LLM into the PPO training loop via the Logit Fusion mechanism.

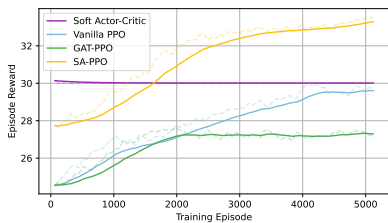


Fig. 9. Training reward curves for different algorithms.

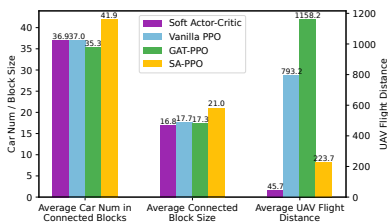


Fig. 10. Comparison of VANET connectivity metrics.

As shown in Fig. 9, SA-PPO demonstrates a convergence speed significantly superior to all baseline algorithms. By leveraging semantic priors provided by the LLM to prune the invalid action space, SA-PPO reaches a stable high-reward state around 2,500 episodes, whereas other baselines require substantially more interactions. The quantitative metrics in Fig. 10 reveal distinct operational patterns among the algorithms. SA-PPO achieves the highest average number of vehicles within the connected component (41.9), surpassing both GAT-PPO and Vanilla PPO. Crucially, SA-PPO achieves this while maintaining an extremely low average UAV flight distance (223.7 m). This indicates that SA-PPO accurately identifies

topologically critical intersections and stations there, moving only when necessary. This stands in sharp contrast to the lazy behavior of SAC (45.7 m), which sacrifices connectivity to save energy, and the inefficient behaviors of other baselines. SA-PPO successfully resolves the multi-objective optimization problem, achieving maximum connectivity coverage with minimal energy consumption.

It should be noticed in Fig. 9 and Fig. 10 that despite employing a Graph Neural Network (GNN), GAT-PPO performs comprehensively worse than the simple Vanilla PPO. Not only is its connectivity performance inferior, but its energy consumption increases drastically, with a flight distance reaching 1158.2 m, which is nearly 1.5 times that of Vanilla PPO and more than 5 times that of SA-PPO. We attribute this to the graph attention mechanism’s hypersensitivity to local traffic noise. In scenarios with static road network topology but fluctuating vehicle density, the GAT-based agent fails to filter out transient noise, leading to unstable and continuous blind maneuvering between adjacent nodes in pursuit of fleeting traffic hotspots. This behaviour results in excessive energy waste without forming a stable coverage structure. In contrast, the simple MLP-based Vanilla PPO is less susceptible to such over-smoothing and jitter, thus outperforming GAT-PPO. This underscores the value of our SA-PPO approach. Rather than enhancing performance by increasing the complexity of the feature extractor, we guide the agent toward global optimality and policy stability by injecting stable semantic common sense via the LLM.

Furthermore, to qualitatively analyze the decision-making logic, we visualize the UAV trajectories generated by different algorithms in simulation snapshots, as shown in Fig. 11. SA-PPO exhibits a highly intelligent “Strategic Stationing” pattern. The trajectory shows the UAV flying directly to critical cut-vertex intersections in the road network and maintaining a precise hover. This decision-making behavior aligns perfectly with its extremely low flight distance (i.e. 223.7 m). Guided by LLM semantic priors, the agent confidently ignores transient traffic noise in fringe areas and anchors itself to global connectivity hubs, thereby achieving maximum connectivity enhancement with minimal energy expenditure. The trajectory of Vanilla PPO appears chaotic and lacks strategic direction, often wandering in low-density edge regions. Consistent with the quantitative data, the SAC agent remains nearly static, confirming the issue of Mode Collapse. These visualizations confirm that the common sense injected by the LLM is successfully translated into spatially rational flight patterns.

2) *Ablation Studies*: To strictly verify the contribution of semantic priors and the effectiveness of the Logit Fusion mechanism, we conduct ablation studies by comparing the proposed SA-PPO with two variants:

- 1) **w/o LLM (Vanilla PPO)**: The semantic branch is removed, and the agent learns solely through the PPO Actor. This serves as a benchmark for blind exploration.
- 2) **w/o Logit Fusion (Pure Semantic Policy)**: The RL branch is removed, and actions are selected by directly sampling from the fine-tuned LLM output distribution ($a \sim \text{Softmax}(z_{LLM})$). This variant is used to evaluate

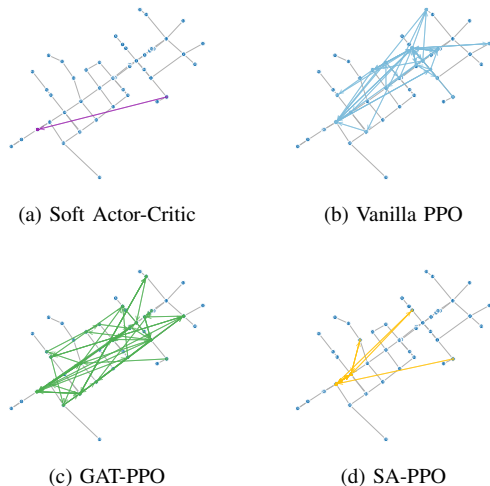


Fig. 11. UAV trajectory visualization under different algorithms.

the quality of the raw semantic priors without RL adaptation.

The comparative results are summarized in Fig. 12. The w/o Logit Fusion variant achieved a significantly higher connectivity score than Vanilla PPO. This result proves that the fine-tuned LLM has successfully internalized the topological “common sense” of the urban road network. Even without any interaction-based reinforcement learning, the domain knowledge embedded in the LLM outperforms the policy learned by the standard DRL agent through trial and error, thereby validating the necessity of the knowledge alignment phase. However, the pure semantic policy reveals a fatal flaw regarding energy consumption. As shown in Fig. 12, the pure semantic policy exhibits an extremely high flight distance (980.6 m). This reflects the myopia of the LLM, which continuously moves between various optimal intersections without considering energy penalties. In contrast, SA-PPO achieves the optimal balance. It obtains the highest connectivity (41.9) with the lowest flight distance (223.7 m). This demonstrates the value of the Logit Fusion mechanism, in which the PPO component effectively constrains the hyperactive tendencies of the LLM, teaching the agent to perform strategic stationing at key nodes identified by the LLM, rather than blindly patrolling.

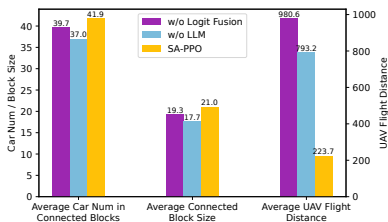


Fig. 12. Ablation study results comparing SA-PPO with its variants.

3) **Robustness and Generalization:** To evaluate the robustness of the algorithms against temporal distribution shifts in traffic patterns, all models are trained using traffic flow data starting at 08:20 and tested in six distinct time periods ranging from 08:00 to 18:00 with identical duration. As illustrated in Fig. 13, SA-PPO demonstrates exceptional scenario-adaptive intelligence. In hard sparse scenarios such as 12:00

where connectivity is scarce, it leverages topological priors to achieve a superior connectivity score of 50.3, surpassing Vanilla PPO (44.0) by over 14%. Conversely, in easy dense scenarios such as 16:00, it adopts a rational trade-off strategy. While maintaining a competitive connectivity level (79.4 vs 86.2), it reduces energy consumption by approximately 50% (471.3 m vs 954.0 m) compared to the hyperactive Vanilla PPO. Furthermore, SA-PPO exhibits dynamic maneuverability, capable of dynamically adjusting its flight distance from 152.1 m at 14:00 to 471.3 m at 16:00 according to real-time traffic demands, thereby proving its ability to effectively generalize to unseen traffic distributions.

V. CONCLUSION

To address the fragmentation issue of VANETs in complex urban environments, we proposed the SA-DRL framework, effectively overcoming the limitations of blind exploration and sample inefficiency in traditional methods caused by a lack of topological semantic understanding. In this work, we quantified network fragmentation using RTG and DCG, and designed a four-stage pipeline incorporating the SA-PPO algorithm. This architecture integrated the reasoning capabilities of LLMs as semantic priors into policy learning via a Logit Fusion mechanism. Simulation experiments based on real-world trajectories demonstrated that our method effectively avoided the Mode Collapse issue observed in the Soft Actor-Critic algorithm. Furthermore, compared to the Vanilla PPO baseline, SA-PPO not only exhibited stronger generalization capabilities against dynamic traffic flows but also achieved convergence using only 26.6% of the training episodes, reducing UAV energy consumption to 28.2% while improving two key connectivity metrics by 13.2% and 23.5%, respectively.

REFERENCES

- [1] V.-L. Nguyen, R.-H. Hwang, P.-C. Lin, A. Vyas, and V.-T. Nguyen, “Toward the age of intelligent vehicular networks for connected and autonomous vehicles in 6G,” *IEEE Network*, vol. 37, no. 3, pp. 44–51, 2023.
- [2] M. J. N. Mahi, S. Chaki, S. Ahmed, M. Biswas, M. S. Kaiser, M. S. Islam, M. Sookhak, A. Barros, and M. Whaiduzzaman, “A review on VANET research: Perspective of recent emerging technologies,” *IEEE Access*, vol. 10, pp. 65 760–65 783, 2022.
- [3] T. Abbas, K. Sjöberg, J. Karedal, and F. Tufvesson, “A measurement based shadow fading model for vehicle-to-vehicle network simulations,” *Int. J. Antennas Propag.*, vol. 2015, no. 1, p. 190607, 2015.
- [4] N. Akhtar, S. C. Ergen, and O. Ozkasap, “Vehicle mobility and communication channel models for realistic and efficient highway vanet simulation,” *IEEE Trans. Veh. Technol.*, vol. 64, no. 1, pp. 248–262, 2015.
- [5] O. S. Oubbati, M. Atiquzzaman, A. Baz, H. Alhakami, and J. Ben-Othman, “Dispatch of UAVs for urban vehicular networks: A deep reinforcement learning approach,” *IEEE Trans. Veh. Technol.*, vol. 70, no. 12, pp. 13 174–13 189, 2021.
- [6] M. Lehsaini, N. Gaouar, and T. Nebbou, “Efficient deployment of roadside units in vehicular networks using optimization methods,” *Int. J. Commun. Syst.*, vol. 35, no. 14, p. e5265, 2022.
- [7] J. Clancy, D. Mullins, B. Deegan, J. Horgan, E. Ward, C. Eising, P. Denny, E. Jones, and M. Glavin, “Wireless access for V2X communications: Research, challenges and opportunities,” *IEEE Commun. Surv. Tutorials*, vol. 26, no. 3, pp. 2082–2119, 2024.
- [8] H. Kurunathan, H. Huang, K. Li, W. Ni, and E. Hossain, “Machine learning-aided operations and communications of unmanned aerial vehicles: A contemporary survey,” *IEEE Commun. Surv. Tutorials*, vol. 26, no. 1, pp. 496–533, 2024.

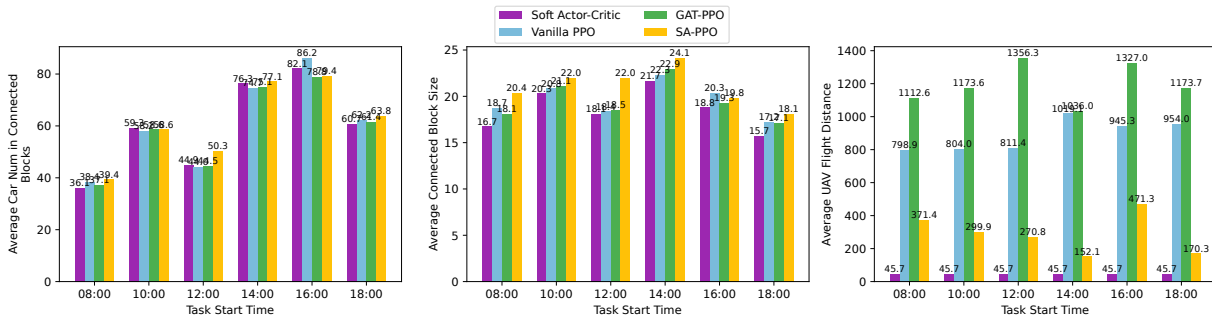


Fig. 13. Ablation study results comparing SA-PPO with its variants.

- [9] M. Gapeyenko, D. Moltchanov, S. Andreev, and R. W. Heath, "Line-of-sight probability for mmwave-based UAV communications in 3D urban grid deployments," *IEEE Trans. Wireless Commun.*, vol. 20, no. 10, pp. 6566–6579, 2021.
- [10] J. Sabzehali, V. K. Shah, Q. Fan, B. Choudhury, L. Liu, and J. H. Reed, "Optimizing number, placement, and backhaul connectivity of multi-UAV networks," *IEEE Internet Things J.*, vol. 9, no. 21, pp. 21 548–21 560, 2022.
- [11] H. S. Yahia and A. S. Mohammed, "Path planning optimization in unmanned aerial vehicles using meta-heuristic algorithms: A systematic review," *Environ. Monit. Assess.*, vol. 195, no. 1, p. 30, 2023.
- [12] Y. Bai, H. Zhao, X. Zhang, Z. Chang, R. Jäntti, and K. Yang, "Toward autonomous multi-UAV wireless network: A survey of reinforcement learning-based approaches," *IEEE Commun. Surv. Tutorials*, vol. 25, no. 4, pp. 3038–3067, 2023.
- [13] J. Schulman, F. Wolski, P. Dhariwal, A. Radford, and O. Klimov, "Proximal policy optimization algorithms," *arXiv preprint arXiv:1707.06347*, 2017.
- [14] Y. Guan, S. Zou, H. Peng, W. Ni, Y. Sun, and H. Gao, "Cooperative UAV trajectory design for disaster area emergency communications: A multiagent PPO method," *IEEE Internet Things J.*, vol. 11, no. 5, pp. 8848–8859, 2024.
- [15] S. Javaid, H. Fahim, B. He, and N. Saeed, "Large language models for UAVs: Current state and pathways to the future," *IEEE Open J. Veh. Technol.*, vol. 5, pp. 1166–1192, 2024.
- [16] L. Yuan, C. Deng, D.-J. Han, I. Hwang, S. Brunswicker, and C. G. Brinton, "Next-generation llm for uav: From natural language to autonomous flight," *arXiv preprint arXiv:2510.21739*, 2025.
- [17] S. Bubeck, V. Chandrasekaran, R. Eldan, J. Gehrke, E. Horvitz, E. Kamar, P. Lee, Y. T. Lee, Y. Li, S. Lundberg *et al.*, "Sparks of artificial general intelligence: Early experiments with gpt-4," *arXiv preprint arXiv:2303.12712*, 2023.
- [18] W. Zu, W. Song, R. Chen, Z. Guo, F. Sun, Z. Tian, W. Pan, and J. Wang, "Language and sketching: An LLM-driven interactive multimodal multi-task robot navigation framework," in *2024 IEEE Int. Conf. Robot. Autom. (ICRA)*, 2024, pp. 1019–1025.
- [19] S. Mokhtari, N. Nouri, J. Abouei, A. Avokh, and K. N. Plataniotis, "Relaying data with joint optimization of energy and delay in cluster-based uav-assisted VANETs," *IEEE Internet Things J.*, vol. 9, no. 23, pp. 24 541–24 559, 2022.
- [20] O. Chughtai, N. N. Qadri, Z. Kaleem, and C. Yuen, "Drone-assisted cooperative routing scheme for seamless connectivity in V2X communication," *IEEE Access*, vol. 12, pp. 17 369–17 381, 2024.
- [21] A. Andreou, C. X. Mavromoustakis, J. M. Batalla, E. K. Markakis, and G. Matorakis, "Uav-assisted RSUs for V2X connectivity using voronoi diagrams in 6G+ infrastructures," *IEEE Trans. Intell. Transp. Syst.*, vol. 24, no. 12, pp. 15 855–15 865, 2023.
- [22] X. Fan, H. Zhang, Y. Huang, Y. Su, H. Li, J. Huo, C. Sun, S. Hao, and L. Zhen, "Temporal data dissemination in UAV-assisted VANETs through time-varying graphs," *IEEE Trans. Veh. Technol.*, vol. 73, no. 10, pp. 14 835–14 846, 2024.
- [23] X. Wei, L. Cai, N. Wei, P. Zou, J. Zhang, and S. Subramaniam, "Joint UAV trajectory planning, DAG task scheduling, and service function deployment based on DRL in uav-empowered edge computing," *IEEE Internet Things J.*, vol. 10, no. 14, pp. 12 826–12 838, 2023.
- [24] Y. Yao, K. Lv, S. Huang, and W. Xiang, "3D deployment and energy efficiency optimization based on DRL for RIS-assisted air-to-ground communications networks," *IEEE Trans. Veh. Technol.*, vol. 73, no. 10, pp. 14 988–15 003, 2024.
- [25] J. Chen, D. Huang, Y. Wang, Z. Yu, Z. Zhao, X. Cao, Y. Liu, T. Q. S. Quek, and D. Oliver Wu, "Enhancing routing performance through trajectory planning with DRL in UAV-aided VANETs," *IEEE Trans. Mach. Learn. Commun. Netw.*, vol. 3, pp. 517–533, 2025.
- [26] P. Hou, Y. Huang, H. Zhu, Z. Lu, S.-C. Huang, Y. Yang, and H. Chai, "Distributed DRL-based intelligent over-the-air computation in unmanned aerial vehicle swarm-assisted intelligent transportation system," *IEEE Internet Things J.*, vol. 11, no. 21, pp. 34 382–34 397, 2024.
- [27] H. Samma and S. El-Ferik, "UAV visual path planning using large language models," *Transp. Res. Procedia*, vol. 84, pp. 339–345, 2025.
- [28] S. Cai, Y. Wu, and L. Zhou, "LLM-land: Large language models for context-aware drone landing," *arXiv preprint arXiv:2505.06399*, 2025.
- [29] Q. Zhou, J. Wu, M. Zhu, Y. Zhou, F. Xiao, and Y. Zhang, "LLM-QL: A LLM-enhanced q-learning approach for scheduling multiple parallel drones," *IEEE Trans. Knowl. Data Eng.*, vol. 37, no. 9, pp. 5393–5406, 2025.
- [30] J. Wu, H. You, B. Sun, and J. Du, "LLM-driven pareto-optimal multi-mode reinforcement learning for adaptive UAV navigation in urban wind environments," *IEEE Access*, vol. 13, pp. 163 550–163 570, 2025.
- [31] S. Albeaik, A. Bayen, M. T. Chiri, X. Gong, A. Hayat, N. Kardous, A. Keimer, S. T. McQuade, B. Piccoli, and Y. You, "Limitations and improvements of the intelligent driver model (IDM)," *SIAM J. Appl. Dyn. Syst.*, vol. 21, no. 3, pp. 1862–1892, 2022.
- [32] A. Al-Hourani, S. Kandeepan, and S. Lardner, "Optimal LAP altitude for maximum coverage," *IEEE Wireless Commun. Lett.*, vol. 3, no. 6, pp. 569–572, 2014.
- [33] Y. Ding, Q. Zhang, W. Lu, N. Zhao, A. Nallanathan, X. Wang, and X. Yang, "Collaborative communication and computation for secure UAV-enabled MEC against active aerial eavesdropping," *IEEE Trans. Wireless Commun.*, vol. 23, no. 11, pp. 15 915–15 929, 2024.
- [34] W. Yuan, G. Cao, Y. Hou, J. Wang, S. Chen, H. He, and J. Yang, "Deep transfer reinforcement learning based exploration enhanced multi-UAV trajectory planning," *IEEE Trans. Commun.*, pp. 1–1, 2025.
- [35] J. He, M. Rungta, D. Koleczek, A. Sekhon, F. X. Wang, and S. Hasan, "Does prompt formatting have any impact on LLM performance?" *arXiv preprint arXiv:2411.10541*, 2024.
- [36] E. J. Hu, Y. Shen, P. Wallis, Z. Allen-Zhu, Y. Li, S. Wang, L. Wang, W. Chen *et al.*, "Lora: Low-rank adaptation of large language models," *ICLR*, vol. 1, no. 2, p. 3, 2022.
- [37] F. Yu, H. Yan, R. Chen, G. Zhang, Y. Liu, M. Chen, and Y. Li, "City-scale vehicle trajectory data from traffic camera videos," *Sci. Data*, vol. 10, no. 1, p. 711, Oct 2023. [Online]. Available: <https://doi.org/10.1038/s41597-023-02589-y>
- [38] Y. Zheng, R. Zhang, J. Zhang, Y. Ye, Z. Luo, Z. Feng, and Y. Ma, "Llamafactory: Unified efficient fine-tuning of 100+ language models," in *Proc. 62nd Annu. Meeting Assoc. Comput. Ling. (ACL)*. Bangkok, Thailand: Association for Computational Linguistics, 2024. [Online]. Available: <http://arxiv.org/abs/2403.13372>
- [39] W. Kwon, Z. Li, S. Zhuang, Y. Sheng, L. Zheng, C. H. Yu, J. E. Gonzalez, H. Zhang, and I. Stoica, "Efficient memory management for large language model serving with pagedattention," in *Proc. 29th ACM Symp. Oper. Syst. Princ. (SOSP)*, 2023.
- [40] S. Goudarzi, S. Ahmad Soleymani, M. Hossein Anisi, A. Jindal, and P. Xiao, "Optimizing UAV-assisted vehicular edge computing with age of information: An SAC-based solution," *IEEE Internet Things J.*, vol. 12, no. 5, pp. 4555–4569, 2025.